International Journal of Thermal Science, 2015, Vol. 88, pp. 136–147.

Numerical Investigation of Conjugated Heat Transfer in a Channel with a Moving Depositing Front

H.Y. Li[1*], Y.F. Yap[2], J. Lou[1], J.C. Chai[2], Z. Shang[1]

[1]Institute of High Performance Computing, Agency for Science, Technology and Research (A*STAR), 1 Fusionopolis Way,

16-16 Connexis, Singapore 138632, Singapore

[2]Department of Mechanical Engineering, The Petroleum Institute,
Abu Dhabi, United Arab Emirates

Abstract

This article presents numerical simulations of conjugated heat transfer in a fouled channel with a moving depositing front. The depositing front separating the fluid and the deposit layer is captured using the level-set method. Fluid flow is modeled by the incompressible Navier-Stokes equations. Numerical solution is performed on a fixed mesh using the finite volume method. The effects of Reynolds number and thermal conductivity ratio between the deposit layer and the fluid on local Nusselt number as well as length-averaged Nusselt number are investigated. It is found that heat transfer performance, represented by the local and length-averaged Nusselt number reduces significantly in a fouled channel compared with that in a clean channel. Heat transfer performance decreases with the growth of the deposit layer. Increase in Reynolds, Prandtl numbers or both enhances heat transfer. Besides, heat transfer is enhanced when the thermal conductivity ratio between the deposit layer and the fluid is lower than 20 but it decreases when the thermal conductivity ratio is larger than 20.

Keywords: Conjugated heat transfer, Moving depositing front, Level-set method, Nusselt number.

[*] Corresponding author: Tel: +65-6419-1315.

E-mail address: lih@ihpc.a-star.edu.sg

Nomenclature

C	particle concentration (kg/m^3)
c_p	specific heat (J/kgK)
D	diffusion coefficient (m^2/s)
f	friction coefficient
H	height of domain (m)
$H(\phi)$	smoothed heaviside function
k	thermal conductivity (W/mK)
r_d	reaction rate for deposition (m/s)
L	length of domain (m)
Nu	Nusselt number
$\hat{n}$	unit normal at the interface
$\vec{q}$	deposition flux (kg/ m^{2}s)
p	pressure (Pa)
Pr	Prandtl number
Re	Reynolds number
$\overline{\text{sign}}(\phi)$	Sign function
S	signum fuction
T	temperature (^{o}C)
t	time (s)
$\bar{t}$	pseudo time (s)
$\vec{u}$	velocity vector (m/s)
u_t	tangential velocity (m/s)
x,y	Cartesian coordinate
Δx	mesh size (m)

Greek Symbols

δ	height of the deposit region (m)
$\delta(\phi)$	Dirac delta function
$\tilde{\Gamma}$	diffusion coefficient (m^2/s)
θ	dimensionless temperature
ϕ, ϕ'	level set function (m)
φ	component of $\vec{u}_{i,ext}$
ε	interface thickness (m)
μ	dynamic viscosity (kg/m·s)
ρ	density (kg/m^3)

τ	shear stress (Pa)
Ω	domain of interest

Subscripts

b	bulk
d	deposit
i	interface
i,ext	extension velocity
in	inlet
out	outlet
w	wall
+	fluid region
-	deposit region
*	dimensionless
0	initial status

1 Introduction

Conjugated heat transfer in a channel with a deposit layer gradually growing on the wall is widely encountered in many engineering applications such as fouling in heat exchangers [1-4]. In these systems, the working fluid carries particles either of an organic or inorganic origin flowing into channels. These particles have a tendency to deposit onto the wall of the channels, forming a deposit layer. The continuously growing and increasingly thicker deposit layer, formed by the deposited particles, normally has a low thermal conductivity. With heat transfer involved, such deposit layer introduces extra thermal resistance and consequently leads to a low heat transfer performance of the system. Besides, the deposit layer reduces flow cross sectional area of the channel and directly responsible for inducing a larger pressure drop. Unfortunately, the deposition process, although highly undesirable for heat transfer, can only be minimized. Therefore, such kind of system normally operates with a formed deposit layer of a tolerable

thickness. As such, a good understanding of the conjugated heat transfer coupling the evolving deposit layer and fluid flow is important.

Conjugated heat transfer with a moving depositing front can be investigated experimentally. Nuntaphan and Kiatsiriroat [1] studied the effect of fly ash on the heat transfer performance of a heat exchanger with spiral finned-tubes. They found that the thermal resistance caused by the fouling of the fly ash increases with time in the testing period of 8 hours. The growing of silica deposition in a heat exchanger during combustion of siloxane with gas was experimentally studied by Turkin et al. [2]. Their results showed that particle distribution of the silica had no much effect on the deposition flux. However, the deposition flux of silica increases linearly with the siloxane concentration in the mixture. Li et al. [3] investigated fouling in corrugated heat exchangers. They found that increase of inlet fluid velocity reduces fouling resistance. Fouling in a twisted tube heat exchanger is studied by Al-Hadhrami et al. [4]. Their results showed that the heat input had significant effect on fouling resistance when the inlet fluid velocity was low. Genić et al. [5] investigated fouling in 8 plate heat exchangers. They found that fouling depends strongly on the fluid velocity. Wax deposition in a crude oil pipeline system was studied by Valinejad and Nazar [6]. It was shown that a waxy crude oil with high wax content resulted in more solid wax deposited on the walls. Zhang et al. [7] conducted experimental and theoretical investigations of fouling on four corrugated plate heat exchangers. The effects of plate height, plate spacing and plate angle on the fouling process were studied. They concluded that the plate heat exchanger with the largest diameter and height to pitch ratio gave the best antifouling performance. Their theoretical results agreed well with the experimental data. Malayeri et al. [8] studied the influence of fouling under pool boiling process. They found that the increase of bubble formation reduces fouling. Generally, experimental study may involve large time scale.

One of the examples is fouling in heat exchangers. Fouling of heat exchanger can occur in weeks, months, years or even longer. Once the heat exchanger is fouled, cleaning process is necessary. Physical cleaning generally involves dismantling and reassembling of the equipment. In certain industries, chemicals can be used to remove the deposit. If not performed properly, these cleaning processes will inevitably damage the equipment and thus shorten the life of the equipment. Therefore, the cost for experimental study of fouling could be substantial. Occasionally, experiments demand extreme cautiousness because of high pressure and hazardous chemical materials. In view of this, theoretical investigations, especially numerical simulations, play an important role in understanding conjugated heat transfer with a moving depositing front.

The channel with a moving depositing front is generally divided into two regions, i.e. a fluid region and a deposit region formed by the deposited solid particles. In clean channels where no particle deposit on the walls; heat is directly transferred to the incoming fluid in the form of convection heat transfer between the hot surface and the incoming fluid. However, with particle deposition formed on the wall of the channel, heat has to be conducted first through the additional deposit layer from hot wall to the depositing front. Then the incoming fluid carries the heat downstream. From a modeling point of view, this kind of problem is governed by conservation equations for mass, momentum, species and energy, coupled with the appropriate interfacial condition at the depositing front separating the fluid from the deposit layer. In particular, the depositing front is a moving boundary. All of these should be incorporated in the numerical model so that the heat transfer with a moving depositing front can be studied more realistically especially when the deposit layer is not thin relative to the characteristic length. Giving the difficulties in capturing the moving depositing front, most of the existing numerical works are based on a known fixed depositing front. Sunden [9] studied the conjugated heat

transfer in a circular cylinder with a heated core inside. The heat core is assumed to be the deposit layer. It is found that thermal conductivity ratio between the deposit layer and fluid has significant effect on the heat transfer. Owen et al. [10] investigated the thermal resistance of the deposit layer on the surface of the tube in heat exchanger without considering fluid flow. Their results show that heat transfer can increase or decrease depending on the thickness of the deposit layer as well as its thermal conductivity. Brahim et al. [11] simulated heat transfer in deposition process with a fictitious growth rate of the crystal deposit. Thermal resistance caused by the growth of the crystals was predicted. Their work is among the first which consider the depositing front as a moving boundary. However, simplification of a simple geometry for the depositing front is assumed. Their model can be modified to capture the actual growth of the crystal more precisely. Heat transfer performance of fouling cross-flow heat exchanger is numerically studied by Kaptan et al. [12]. The deposit layer due to fouling is assumed to be concentric or eccentric to the tube of the heat exchanger. Effects of the thermal conductivity and the thickness of the deposit layer on heat transfer coefficient are investigated. It is found that thicker deposit layer reduces the heat transfer rate. A similar study has been done by Vessakosol and Charoensuk [13] who investigated effect of Prandtl number and thermal conductivity ratio between fluid and deposit layer on heat transfer performance of a heat exchanger. Their results showed that high heat transfer performance was expected for high Reynolds number as well as Prandtl number.

The above mentioned simulation work on the conjugated heat transfer is either considering a fixed depositing front or pseudo simple depositing front. These can be furhter improved by having a dynamocially evolving depositing front. In a channel with a moving depositing front, the deposit layer evolves with time and the depositing rate is generally governed by appropriate deposition kinetics. Therefore, additional calculations based on such phenomenon to capture the

depositing front are necessary. Conjugate heat transfer involving a growing deposit layer, although important, has not been studied sufficiently due to its complexity. This numerical study is undertaken to fill in some of the gaps in this respect. In this work, the level-set method is used to capture the evolving depositing front [15]. Fluid flow is modeled using the incompressible Navier-Stokes equations. Numerical solutions were performed on a fixed mesh using the finite volume method (FVM). A FORTRAN code was developed for the approach presented in this article. The capability of the current model is showcased via examples with fouling in heat exchanger. Effects of Reynolds number (up to 1000), Pr number (up to 1.1) and thermal conductivity ratio of deposit to fluid (up to 100) on the heat transfer performance were investigated.

2. Problem Description

The two-dimensional channel of interest is schematically shown in Fig. 1. Both the upper and the lower walls are maintained at a temperature of T_w. Fluid at a temperature of T_{in} and carrying suspended solid particles flows into the channel at the inlet. These solid particles gradually deposit onto the walls and form deposit layers. The driving force for the particles to deposit onto the surface can either be of a physical, chemical, or a combination of these origins. Deposition/fouling with corrosion occur simultaneously is not considered in the current work. Regardless of the origin of the deposition, it can be modelled via a deposition flux of a given functional form. Here in this article, the deposition flux is assumed to be a first order reaction. This functional form can be modified accordingly to incorporate a more general deposition process. Once the deposit layers are formed, the domain can be considered to consist of a fluid region Ω_+ and a deposit region Ω_-. These two regions are separated by the depositing front Γ. The case of $T_w > T_{in}$ is of interest here. Basically, heat is conducted from the hot walls through

the deposit layers and then to the flowing fluid. The increasingly thicker deposit layer introduces extra thermal resistance and affects heat transfer. The effect on heat transfer is quantitatively addressed here in this article.

3. Mathematical Formulation

3.1 Governing Equations

In this study, level-set method is used to capture the evolving depositing front [15]. The level-set function ϕ is defined as the signed short normal distance from the front. Opposite signs are assigned to the two different regions, in particular, $\phi > 0$ for the fluid region and $\phi < 0$ for the deposit region. Of course, the front is then implicitly represented by the zero level-set, i.e. $\phi = 0$. The movement of the front can now be captured by monitoring the evolution of the level-set function governed by

$$\frac{\partial \phi}{\partial t} + \vec{u}_{i,ext} \bullet \nabla \phi = 0, \forall \vec{x} \in \Omega \tag{1}$$

where $\vec{u}_{i,ext}$ is a velocity field extended from the velocity of the depositing front $\vec{u}_i$. The extension is constructed in such a way that $\vec{u}_{i,ext}$ is constant along the curve normal to the depositing front. This can be easily achieved using the approach suggested by [16] as

$$\frac{\partial \varphi}{\partial t} + S(\phi)\hat{n} \bullet \nabla \varphi = 0 \quad , \forall \vec{x} \in \Omega \tag{2a}$$

$$S(\phi) = \begin{cases} -1, & \text{if } \phi < 0 \\ 0, & \text{if } \phi = 0 \\ +1, & \text{if } \phi > 0 \end{cases} \tag{2b}$$

where φ is the velocity component of $\vec{u}_i$. Numerically, ϕ will drift away from a distance function gradually during the iterative numerical solution. To alleviate this problem, redistancing

is introduced [17] whereby the level-set function ϕ is replaced by the "steady-state" solution of a second distance function ϕ' governed by

$$\frac{\partial \phi'}{\partial \bar{t}} + \overline{\text{sign}}(\phi)\left(|\nabla \phi'| - 1\right) = 0 \quad , \forall \vec{x} \in \Omega \tag{3}$$

where $\bar{t}$ is the pseudo time for the variable ϕ'. $\overline{\text{sign}}(\phi)$ is given by

$$\overline{\text{sign}}(\phi) = \frac{\phi}{\sqrt{\phi^2 + |\nabla \phi|^2 \left(\Delta x^2\right)}} \tag{4}$$

The initial condition for Eq. (4) is

$$\phi'(\vec{x}, 0) = \phi(\vec{x}) \tag{5}$$

The deposition process is modeled as a first order deposition reaction with the deposition flux given by

$$\vec{q} = -\rho_{-} \vec{u}_i = -r_d C \hat{n}_i \tag{6}$$

where ρ_{-}, r_d, C and $\hat{n}_i$ are the density of the deposit, the deposition reaction rate, the particle concentration and unit normal vector pointing into the fluid region respectively. Rearrangement of Eq. (6) gives the velocity of the depositing front as

$$\vec{u}_i = \frac{r_d C \hat{n}_i}{\rho_{-}} \quad , \vec{x} \in \Gamma(t) \tag{7}$$

where the unit vector $\hat{n}_i$ is evaluated as

$$\hat{n} = \frac{\nabla \phi}{|\nabla \phi|} \tag{8}$$

The present framework is applicable generally to a general deposition/fouling process as long as the functional form of the deposition flux, i.e. Eq. (6), is known for the interested type of deposition/fouling. For demonstration purpose, the deposition flux is assumed as a first order reaction in this article.

The conservation equations governing the transport of mass, momentum, particle and energy for the problem are given by

$$\nabla \bullet \vec{u} = 0 \tag{9}$$

$$\frac{\partial(\rho\vec{u})}{\partial t} + \nabla \bullet (\rho\vec{u}\vec{u}) = -\nabla p + \nabla \bullet \left[\mu\left(\nabla\vec{u} + \nabla\vec{u}^{T}\right)\right] \tag{10}$$

$$\frac{\partial C}{\partial t} + \nabla \bullet (\vec{u}C) = \nabla \bullet (D\nabla C) - r_d C\delta(\phi)|\nabla\phi| \tag{11}$$

$$\frac{\partial(\rho c_p T)}{\partial t} + \nabla \bullet (\rho c_p \vec{u} T) = \nabla \bullet (k\nabla T) \tag{12}$$

where D, c_p and k are respectively the diffusion coefficient, the specific heat and thermal conductivity.

By introducing a smoothed Heaviside and a smoothed Dirac functions given respectively by

$$H(\phi) = \begin{cases} 0, & \text{if } \phi < -\varepsilon \\ \dfrac{\phi+\varepsilon}{2\varepsilon} + \dfrac{1}{2\pi}\sin\left(\dfrac{\pi\phi}{\varepsilon}\right), & \text{if } |\phi| \le \varepsilon \\ 1, & \text{if } \phi > +\varepsilon \end{cases} \tag{13a}$$

$$\delta(\phi) \equiv \begin{cases} \dfrac{1+\cos[\pi(\phi-\varepsilon)/\varepsilon]}{2\varepsilon}, & \text{if } 0 \le \phi \le 2\varepsilon \\ 0, & \text{otherwise} \end{cases} \tag{13b}$$

The thermo-physical properties in the conservation equations can be evaluated as

$$\rho = H\rho_+ + (1-H)\rho_- \tag{14a}$$

$$\rho c_p = H(\rho c_p)_+ + (1-H)(\rho c_p)_- \tag{14b}$$

$$\mu(\phi) = \begin{cases} \infty, & \text{if } \phi \le 0 \\ \mu_+, & \text{if } \phi > 0 \end{cases} \tag{14c}$$

$$D(\phi) = \begin{cases} 0, & \text{if } \phi \le 0 \\ D_+, & \text{if } \phi > 0 \end{cases} \tag{14d}$$

$$\frac{1}{k} = \frac{H}{k_+} + \frac{1-H}{k_-} \tag{14e}$$

The deposit layer is modeled as an extremely viscous fluid, i.e. a solid. This is easily achievable in the present formulation with the viscosity defined by Eq. (14c). The second term on the RHS of Eq. (11), i.e. $-r_d C\delta(\phi)|\nabla\phi|$, accounts for the amount of particles transformed into deposit at the depositing front and is only non-zero around the depositing front. During the movement of the depositing front via the convection of ϕ through Eq. (1), some of the particles in the immediate adjacency of the depositing front are trapped in the deposit region. If left untreated, the amount of trapped particles in the growing deposit region increases with time. To alleviate this problem, the trapped particles will be redistributed evenly to all other CVs of the fluid region following the approach suggested in [14].

3.2 Initial and Boundary Conditions

The problem is symmetric at $y = H$. Therefore solutions will only be obtained for the lower half of the channel. For each of the case study in the current article, steady state solution for fluid flow and heat transfer in a clean channel is first obtained. These results are then used as the initial condition in the simulation of the conjugated heat transfer with particle deposition. Such simulation process actually reflects the real situation of fouling as fouling of heat exchanger usually starts from a clean channel. The boundary conditions are listed below:

At the inlet ($x = 0$)

$$u = u_{in},\ v = 0,\ T = T_{in}, C = \begin{cases} C_o & ,0.5H \le y \le H \\ 0 & ,\text{otherwise} \end{cases} \tag{15a}$$

At the outlet ($x = L$)

$$\frac{\partial u}{\partial x} = 0,\ v = 0,\ \frac{\partial C}{\partial x} = 0,\ \frac{\partial T}{\partial x} = 0 \tag{15b}$$

At the wall ($y = 0$)

$$\vec{u} = \vec{0},\ \frac{\partial C}{\partial y} = 0,\ T = T_w \tag{15c}$$

At the symmetric plane ($y = H$)

$$\frac{\partial u}{\partial y} = 0,\ v = 0,\ \frac{\partial C}{\partial y} = 0,\ \frac{\partial T}{\partial y} = 0 \tag{15d}$$

3.3 Numerical Method

The conservation equations (Eqs. 9-12) can be recast into a general equation of the form,

$$\frac{\partial(\tilde{\rho}\Phi)}{\partial t} + \nabla \bullet (\tilde{\rho}\vec{u}\Phi) = \nabla \bullet (\tilde{\Gamma}\nabla\Phi) + S \tag{16}$$

where $\tilde{\rho}$, $\tilde{\Gamma}$, and S are the "appropriate" density, diffusion coefficient and source term, respectively. This general equation is solved via FVM. The velocity-pressure coupling was handled with the SIMPLER algorithm [18]. A 2nd order upwind scheme with superbee limiter [19] is used for the convective term and a fully implicit scheme is used for time integration.

The level-set (Eq. 1) and its redistancing equation (Eq. 3) are spatially discretized with WENO5 (5th order Weighted Essential Non-Oscillatory Scheme) [20]. Since it is a 5th order scheme, numerical diffusion is greatly reduced and allow sections of the front with large curvature to be captured more accurately. Besides, no oscillatory behaviours in the solution occur in the even that characteristics merge. TVD-RK2 (Total-Variational-Diminishing 2nd order Runge-Kutta scheme) [21] is employed to ensure numerical stability in the temporal integration of the level-set and its redistancing equations. To reduce the computational effort, the level-set method is implemented in a narrow-band procedure [22] where the level-set function is solved only within a band of certain thickness from the interface.

4. Results and Discussion

Verifications of the present approach for modeling of particle deposition with heat transfer were performed and documented respectively in [14] and [23], and therefore will not be repeated here. Table 1 shows the thermo-physical value for the fluid and deposit used in the simulation. The results will be presented in dimensionless form. For this purpose, the system of governing equations (Eqs. 9-12) can be non-dimensionalized by defining these dimensionless quantities: x-coordinate $x^* = \frac{x}{H}$, y-coordinate $y^* = \frac{y}{H}$, velocity $u^* = \frac{u}{u_{in}}$ and temperature $\theta = \frac{T - T_{in}}{T_w - T_{in}}$.

Then, the problem can be summarily described by the following group of dimensionless parameters: Reynolds number, dimensionless concentration, Peclet number, Damkholer number, diffusivity ratio and Prandlt number, defined respectively as

$$Re = \frac{\rho_+ u_{in} H}{\mu_+} \tag{17a}$$

$$C^* = \frac{C}{\rho_-} \tag{17b}$$

$$Pe = \frac{u_{in} H}{D_+} \tag{17c}$$

$$Da = \frac{r_d H}{D_+} \tag{17d}$$

$$\alpha^* = \frac{k_- / (\rho c_p)_-}{k_+ / (\rho c_p)_+} \tag{17e}$$

$$Pr = \frac{(\rho c_p)_+}{k_+} \tag{17f}$$

In the following simulations, the dimensionless inlet concentration C_{in}^* and Damkholer number Da are fixed at 0.1 and 5, respectively.

4.1 Effect of particle deposition on the heat transfer performance

The first case of interest is that of Re = 300, Pe = 9.495 and $\alpha^* = 2$. The deposit profile obtained on three different meshes: 80 × 20 control volumes (CVs) with Δt = 0.1, 160 × 40 CVs with Δt = 0.05 and 320 × 80 CVs with Δt = 0.025, are shown in Fig. 2. A mesh of 160 × 40 CVs with Δt = 0.05 is sufficient to resolve most of the essential features of the deposit layer. The maximum differences in the thickness of deposit layer between the mesh of 80 × 20 CVs with Δt = 0.1 and that of 160 × 40 CVs with Δt = 0.05, the mesh of 160 × 40 CVs with Δt = 0.05 and that of 320 × 80 CVs with Δt = 0.025 are 3% and 0.8%, respectively. Further examination of the mesh sensitivity is made on the local Nusselt number Nu_x defined in Eq.(19a). It is found that the differences of Nu_x between these consecutively refined meshes are 2.8% and 0.5%, respectively. Therefore, a mesh size of 160 × 40 CVs with Δt = 0.05 is employed in all subsequent cases.

Shown in Fig. 3 are the dimensionless velocity and temperature fields with the deposit profile superimposed. The interface between the fluid region and the deposit region, also known as depositing front, is plotted with a bold solid line. The numbers on the temperature field is the dimensionless temperatures θ. As mentioned before, simulation for particle deposition starts from the steady state solution of flow in a clean channel. Therefore, the dimensionless velocity and temperature fields at t = 0 in Fig. 3 also represents the flow and temperature fields in a clean channel (without particle deposition). Compared with Fig. 3(a) and Figs. 3(b), 3(c) and 3(d), the presence of the deposit layer affects the flow field as well as the temperature field significantly. Its presence changes the flow and temperature fields and results in a deterioration of heat transfer. At t = 0, fluid carrying suspended particles enters the clean channel at the inlet with a uniform velocity. As fluid flows along the channel, the particles deposit onto the walls of the channel gradually, forming a deposit layer. Given the impermeability of the deposit layer, the presence of

the deposit layer changes the flow field by accelerating and deflecting the flow slightly upward. Generally, the deposit layer near the inlet grows faster than that of the downstream and is therefore thickest due to higher particle concentration upstream. With particles deposited along the flow direction, the concentration of the particle decreases downstream. Therefore, the thickness of the deposit layer then decreases along the channel.

Figure 4 shows the variation of the dimensionless concentration for the suspended particles at different times. The dimensionless concentration is mathematically expressed in Eq. (17b). It is obvious that the particle concentration in the fluid changes temporally and spatially. Some of these particles carried by the fluid deposit onto the walls, leading to a reduction of particle concentration in the fluid.

The plots of the dimensionless deposit thickness (normalized against the characteristic length H) at different time in Fig. 5(a) of clearly show this. The friction factor f at different times is also included in Fig. 5(a). f is defined as [24]:

$$f = \frac{8\tau}{\rho u_{in}^2} \tag{18a}$$

where τ is

$$\tau = \mu \nabla u_t \bullet \hat{n} \tag{18b}$$

u_t is the tangential velocity at the deposition front. The local shear stress at the deposition front varies both spatially and temporally. As the deposit grows it is expected the shear stress varies significantly along the channel.

Heat transfer from the wall to the fluid would eventually rely on convective heat transfer occurring at the depositing front. The mere presence of the deposit layer changes the flow field and the strength of convective heat transfer. To quantify this effect, local Nusselt number defined as

$$Nu_x = \frac{(H-\delta)}{T_i - T_b}\left.\frac{\partial T}{\partial y}\right|_{y=\delta} \tag{19a}$$

in introduced where T_i and T_b are respectively the temperature at the depositing front and the bulk temperature. The bulk temperature is given by

$$T_b = \int_{\delta}^{H} |u| T dy \Big/ \int_{\delta}^{H} |u| dy \tag{19b}$$

Figure 5(b) shows the comparison of Nu_x between a clean and a fouled channel. The transient Nu_x in the fouled channel is shown. Generally, the fouled channel consistently has a lower Nu_x than that of a clean channel. With the solid particles deposited onto the wall of the channel, a deposit layer is formed. This deposit layer introduces an additional thermal resistance for the heat to be transferred from the heated wall to the fluid, consequently, leads to a lower heat transfer performance of the system compared with that in clean channel. As time passes, the thickness of the deposit layer increases, resulting in an even lower Nu_x. It is therefore obvious that Nu_x reduces with the increase of time.

4.2 Effect of Reynolds number on the heat transfer performance

Figure 6 shows the dimensionless velocity and temperature fields for Re = 100, Pe = 3.165, and α^* = 2. Re is directly related to the inlet velocity. A smaller Re corresponds to a lower inlet velocity. With a low inlet velocity, the residence time of particles remains in the channel is longer. The more time the particles spend in the channel, the more time it can diffuses to the depositing front and get deposited. This moves the thickest of the deposit layer upstream as compared with that at Re = 300, Pe = 9.495 and α^* = 2. The particle concentration downstream then reduces, leading to a thin deposit layer downstream. The deposit profile at different times is shown in Fig. 7. Such distribution of the deposit layer on the heated wall is not favorable for heat

transfer. Generally, a fluid with low temperature possesses high potential to obsorb heat from the hot surface maintained at a constant temperature. Therefore, a higher heat transfer performance is expected at the inlet region of the channel as the inlet fluid has a low temperature. However, in this case, a thick deposit layer formed near the inlet present a large thermal resistance which hinders heat to be transferred from the heated wall to the inlet cool fluid. This reduces the heat transfer performance significantly.

The transient behavior of fluid flow and heat transfer at a Re of 500, Pe = 15.825 and α^*= 2 are shown in Fig. 8. Although the particle concentration in the entrance region is high, most of these particles do not deposit because of the high inlet fluid velocity. Instead, these particles are carried by the flowing fluid downstream instead of diffusing towards the depositing front. As a result, the leading edge as well as the location with the thickest deposit layer moves downstream. This can be seen from the deposit profile shown in Fig. 9. The increase of inlet velocity increases convection heat transfer in the depositing front between the fluid and deposit regions. Denser isothermals are found near the depositing front which indicates a high heat transfer performance. In the deposit layer, the heat transfer mode is conduction rather than convection. Therefore, the deposit has a relatively constant temperature gradient.

The transient variation of Nu_x at Re = 100, Pe = 3.165 and Re = 500, Pe = 15.825 for α^* = 2 are shown in Figs. 10(a) and 10(b), respectively. Similar to that shown in Fig. 5 for Nu_x at Re = 300, Pe = 9.495, the presence of deposit layer reduces Nu_x significantly. At Re = 500, Nu_x decreases with the growth of the deposit layer. This is not observed at Re = 100, Pe = 3.165. Given the thick deposit layer near the inlet region, a slight difference in Nu_x is found at different times downstream of x^* = 3 at Re = 100, Pe = 3.165. This indicates that the heat transfer performance

deteriorates at the early stage of fouling process. Special attention should therefore be directed to engineering system prone to such behaviors.

The comparisons of δ^* and Nu_x at different Re and Pe are further made at t = 30 s, shown in Fig. 11(a) and 11(b), respectively. High Re number forms a thin deposit layer upstream and a thick deposit layer downstream while a different deposit profile is created at low Re and Pe numbers. Such a deposit layer profile changes heat transfer performance. For example, at x^* = 0.6, the thickness of the deposit layer at Re = 100 is almost 2 times that of Re = 300 and 4 times that of Re = 500. With such large thickness of the deposit layer, Nu_x at Re = 100 is then significantly reduced by 50% and 36% compared with that of Re = 500 and Re = 300, respectively. However, a slight better heat transfer performance is observed at Re = 500 compared to that of Re = 300 and Re = 100 between x^* = 2 and x^* = 3. After that, there is no much difference in the heat transfer performance at these three Reynolds numbers. This is due to the thick deposit layer downstream under high Re number. The thickness of the deposit layer at Re = 500 at x^* = 2.5 is as high as 3.3 times and 1.3 times compared with that of Re = 100 and Re = 300. Such thick deposit layer downstream at high Re number actually presents large thermal resistance, resulting a reduced heat transfer compared with that of thin deposit layer downstream formed at low Re number. As expected, high Re number corresponds to high heat transfer performance in a clean channel.

In addition to the comparison in local Nusselt number Nu_x, the length-averaged Nu number, i.e. Nu_a is also used to evaluate the heat transfer performance at different Re number to characterize the overall heat transfer performance. The length-averaged Nu number Nu_a is obtained from Nu_x number as

$$Nu_a = \frac{\int_0^L Nu_x dx}{L} \quad (18)$$

The variation of Nu_a at different Re number is shown in Fig. 12. With a deposit layer in the fouled channel, Nu_a reduces significantly compared with that of a clean channel. Further growth of the deposit layer leads to a decrease of Nu_a. Generally, Nu_a number shows a relatively linear increase with the increase of Re number.

4.3 Effect of thermal conductivity ratio between the deposit layer and fluid on the heat transfer performance

Effect of thermal conductivity ratio between the deposit layer and the fluid is now discussed. Figure 13 shows the transient behaviours of the temperature fields at Re = 300, Pe = 9.495 and α^*= 20. Since the flow field is uncoupled with the temperature field in the current study, the velocity field can be referred to as Fig. 3 since these two cases have similar flow field. With the increase of α^*, i.e. thermal conductivity of the deposit layer, the thermal resistance introduced by the deposit layer reduces. Therefore, heat is more easily conducted from the heated wall through deposit layer, leading to a small temperature gradient inside of the deposit layer. Upon transferred to the depositing front, the incoming fluid then carries the heat away. On the other hand, the decrease of thermal conductivity of the deposit layer presents large thermal resistance. This results in additional resistance in transferring heat from the wall to the depositing front at low α^* which reduces the heat transfer performance.

Effect of α^* on Nu_x at different times is shown in Fig. 15. Note Nu_x for the clean channel is only taken from the steady state results for comparison purpose. As expected, heat transfer performance is significantly reduced when compared to that of a clean channel. The increase of α^* increases Nu_x at the entrance region. Upon careful examinations of the graphs for different α^*

shown in the zoomed in area in each figure, it is surprising to find that Nu_x at $\alpha^* = 100$ becomes smaller gradually after $x^* = 1$ and it reaches minimum among the testing cases at t = 30 s. Large Nu_x at the entrance region indicates high convection heat transfer, leading to a high temperature of the fluid at the entrance region. With a high temperature fluid flowing downstream, the convection heat transfer is therefore reduced.

Figure 16 shows the temporal variations of Nu_a at different α^*. Note that x-axis is in log scale. Generally, the increase of α^* increases Nu_a which enhances the heat transfer performance. Such enhancement on the heat transfer performance becomes less significant with the increase of the thermal conductivity ratio between the deposit layer and the fluid. It decreases after $\alpha^* = 20$ given the decreased Nu_x discussed above.

4.4 Effect of Pr number on the heat transfer performance

Figure 17 shows the effect of Pr number on Nu_a. Pr number is defined in Eq. (17f). Generally, the increase of Pr number increases the heat transfer performance. Again, the heat transfer performance in a clean channel is much better than that in a fouled channel. With time progresses, the heat transfer performance in the fouled channel reduces due to the increase of the thickness of deposit layer.

5. Concluding Remarks

The present article investigates conjugated heat transfer in a channel with a growing deposit layer. The depositing front is captured by the level-set method. Heat transfer performance is quantified using local Nusselt number as well as length-averaged Nusselt number. It is shown that heat transfer performance is significantly reduced in fouled channel compared with that of a clean channel. With the growth of the deposit layer on the heated wall, heat transfer performance decreases. The increase of length-averaged Nusselt number is found with the increase of Re and

Pr numbers. The length-averaged Nusselt number increases when the thermal conductivity ratio between the deposit layer and the fluid is less than 20.

References

[1] A. Nuntaphan, T. Kiatsiriroat, Thermal behavior of spiral fin and tube heat exchanger having fly ash deposit, Exp. Therm. Fluid Sci. 31 (2007) 1103-1109.

[2] A.A. Turkin, M. Dutka, D.Vainchtein, S. Gersen, V.M.,van Essen, P. Visser, A.V. Mokhov, H.B. Levinsky, J.Th. M.De Hosson, Deposition of SiO2 nanoparticles in heat exchanger during combustion of biogas, Appl. Energy 113 (2014) 1141-1148.

[3] W. Li, H.X. Li, G.Q. Li, S.C. Yao, Numerical and experimental analysis of composite fouling in corrugated plate heat exchangers, Int. J. Heat Mass Transfer 63 (2013) 351-360.

[4] L.M. Al-Hadhrami, A. Ahmad, A. Al-Qahtani, Experimental study of fouling resistance in twisted tube heat exchanger, Heat Transfer Eng. 33 (2012) 1024-1032.

[5] S, B. Genić, B.M. Jaćimović, D. Mandić, D. Petrović, Experimental determination of fouling factor on plate heat exchangers in district heating system, Energy Build. 50 (2012) 204–211.

[6] R. Valinejad, Ali R. S. Nazar, An experimental design approach for investigating the effects of operating factors on the wax deposition in pipelines, Fuel 106 (2013) 843-850.

[7] G. M. Zhang, G. Q. Li, W. Li, Z. Y. Zhang, X. L. Leng, M. C. Tian, Particle fouling and composite fouling assessment in corrugated plate heat exchangers, Int. J. Heat Mass Transfer 60 (2013) 263-273.

[8] M.R. Malayeri, H. Muller-Steinhagen, M. Jamialahmadi, Fouling of tube bundles under pool boiling conditions, Chem. Eng. Sci. 60 (2005) 1503-1513.

[9] B. Sunden, Conjugated heat transfer from circular cylinders in low Reynolds number flow, Int. J. Heat Mass Transfer 23 (1980) 1359-1367.

[10] I. Owen, E. Buyruk, H. Barrow, Theoretical analysis of the thermal resistance of non-uniform fouling on cross-flow heat exchanger tubes, Appl. Therm. Eng. 16 (1996) 43-50.

[11] F. Brahim, W. Augustin, M. Bohnet, Numerical simulation of the fouling process, Int. J. Therm. Sci. 42 (2003) 323-334.

[12] Y. Kaptan, E. Buyruk, A. Ecder, Numerical investigation of fouling on cross-flow heat exchanger tubes with conjugated heat transfer approach, Int. Commun. Heat Mass Transfer 34 (2008) 1153-1158.

[13] P. Vessakosol, J. Charoensuk, Numerical analysis of heat transfer and flow field around cross-flow heat exchanger tube with fouling, Appl. Therm. Eng. 30 (2010) 1170-1178.

[14] Y.F.Yap, F.M. Vargas, J.C. Chai, A level-set method for convection-diffusive particle deposition, Appl. Math. Model. 37 (2013) 5245-5259.

[15] S. Osher and J.A. Sethian, Fronts propagating with curvature-dependent speed: Algorithms based on Hamilton-Jacobi formulations, J. Comput. Phys. 79 (1988) 12-49.

[16] S. Chen, B. Merriman, S. Osher, P. Smereka, A simple level set method for solving Stefan problems, J. Comput. Phys. 135 (1997) 8-29.

[17] M. Sussman, P. Smereka, S. Osher, A level set approach for computing solutions to incompressible two-phase flow, J. Comput. Phys. 114 (1994) 146-159.

[18] S. V. Patankar, Numerical Heat Transfer and Fluid Flow. Hemisphere Publisher, New York, 1980.

[19] H.K. Versteeg, W. Malalasekera, An Introduction to Computational Fluid Dynamics: The Finite Volume Method, 2nd ed., Prentice Education Limited, England, 2007.

[20] G. S. Jiang, D. Peng, Weighted ENO schemes for Hamilton–Jacobi equations, SIAM J. on Sci. Comput. 21 (2000) 2126-2143.

[21] C. W. Shu, S. Osher, Efficient Implementation of Essentially Non-Oscillatory Shock Capturing Schemes, J. Comput. Phys. 77 (1988) 439-471.

[22] D. Peng, B. Merriman, S. Osher, H. Zhao, M. Kang, A PDE-based fast local level-set method, J. Comput. Phys. 155 (1999) 410-438.

[23] H.Y. Li, K.C. Leong, L.W. Jin, J.C. Chai, Analysis of fluid flow and heat transfer in a channel with staggered porous blocks, Int. J. Therm. Sci. 49 (2010) 950 – 962.

[24] L. T., Bergman, A.S. Lavine, F. P. Incropera, D. P. De Witt, Introduction to Heat Transfer, 6th ed., Wiley, New York, 2011.

Table 1 Thermo-physical values of the fluid and deposit layer

	ρ (kg/m^3)	c_p (J/kgK)	μ (kg/m·s)	k (W/mK)
Fluid	1.0	(1.0~5.0)	2.14×10^{-3}	0.01
Deposit layer	1.0	(1.0~5.0)	∞	(0.005~1)

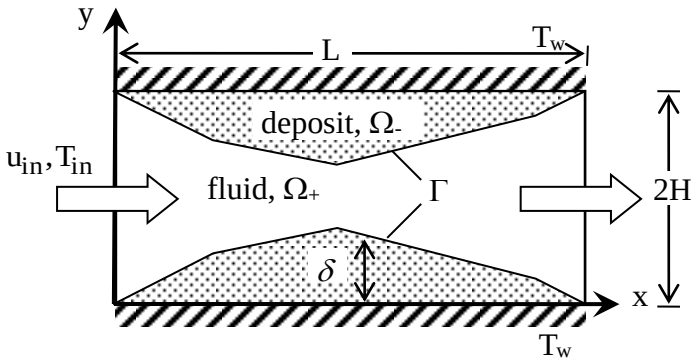

Fig. 1 Schematic of a two-dimensional channel.

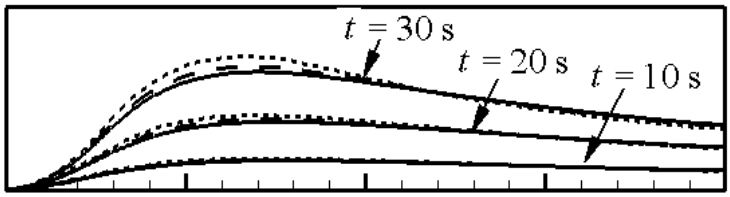

Fig. 2 Deposit profile obtained using 80 × 20 CVs, Δt = 0.1 s (·····), 160 × 40 CVs, Δt = 0.05 s (– –) and 320 × 80 CVs, Δt = 0.025 s (——).

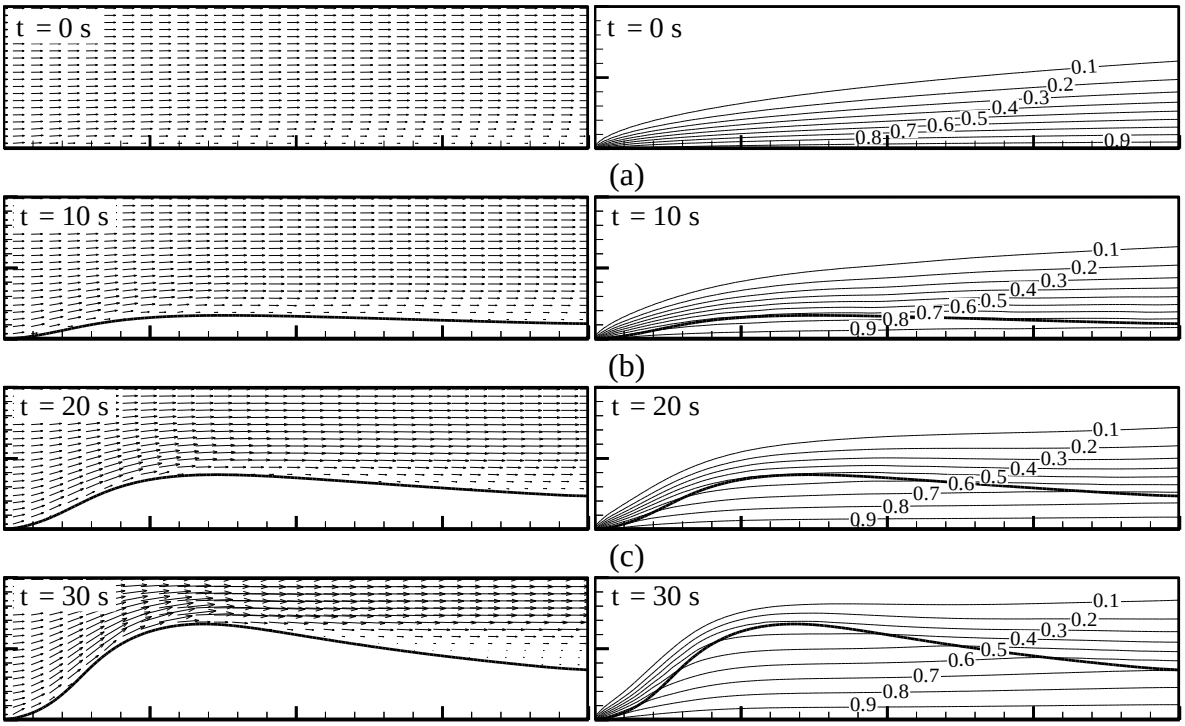

Fig. 3 Dimensionless velocity and temperature fields for Re = 300, Pe = 9.495, α^* = 2, Pr = 0.214 in the fouled channel at (a) t = 0, (b) t = 10 s, (c) t = 20 s, and (d) t = 30 s.

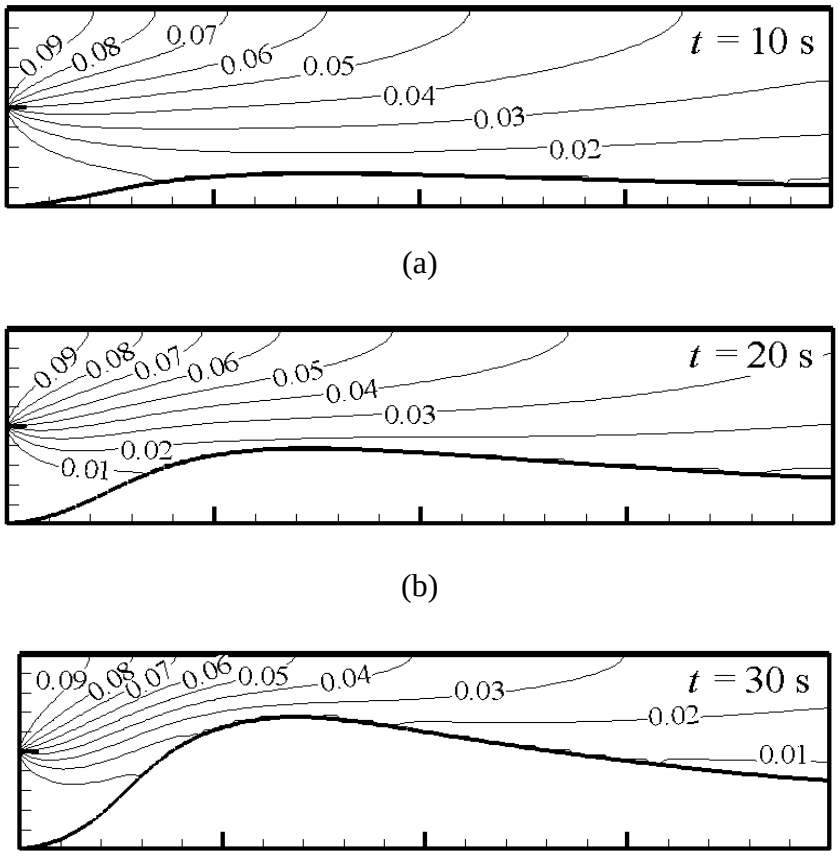

Fig. 4 Dimensionless concentration fields for Re = 300, Pe = 9.495, α^* = 2, Pr = 0.214 in the fouled channel at (a) t = 10 s, (c) t = 20 s, and (d) t = 30 s.

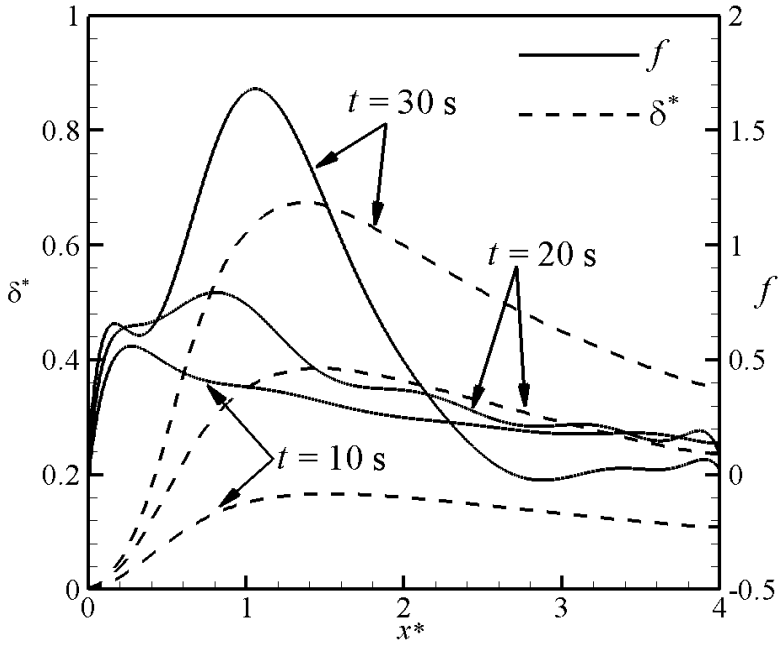

(a)

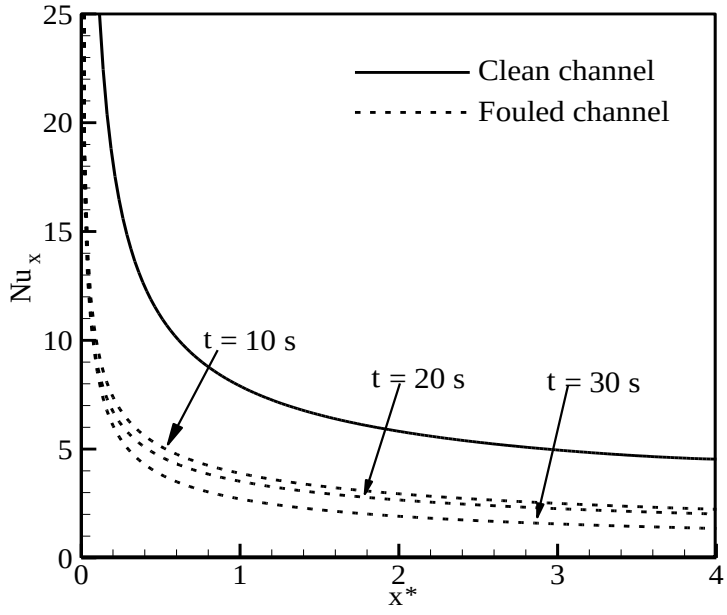

(b)

Fig. 5 Evolution of (a) the deposition profile and friction factor, and (b) Nu_x along the channel for Re = 300, Pe = 9.495, α^* = 2 and Pr = 0.214.

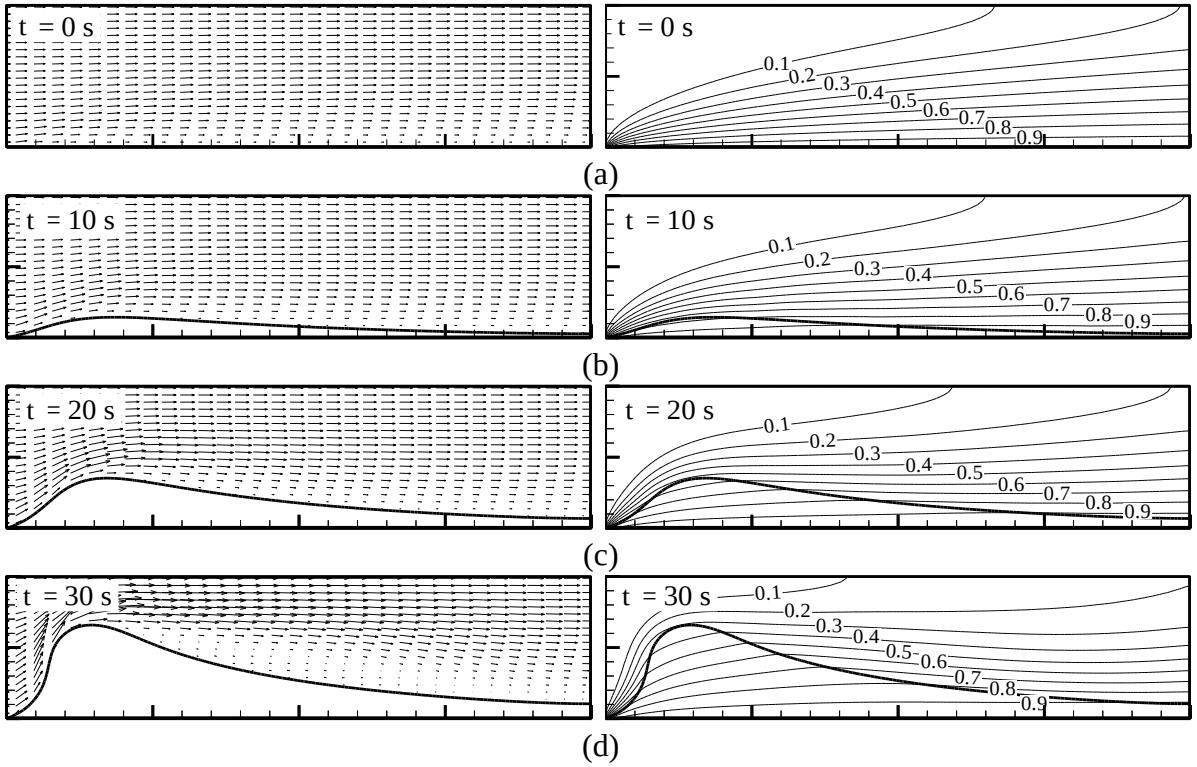

Fig. 6 Dimensionless velocity and temperature fields for the case of Re = 100, Pe = 3.165, α^* = 2 and Pr = 0.214 in the fouled channel at (a) t = 0, (b) t = 10 s, (c) t = 20 s, and (d) t = 30 s.

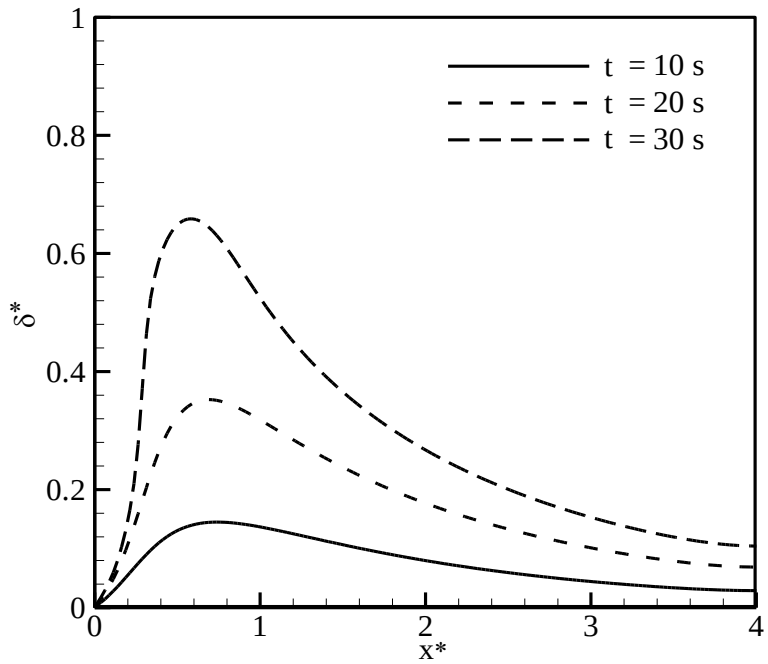

Fig. 7 Evolution of the deposition profile for Re = 100, Pe = 3.165, α^* = 2 and Pr = 0.214.

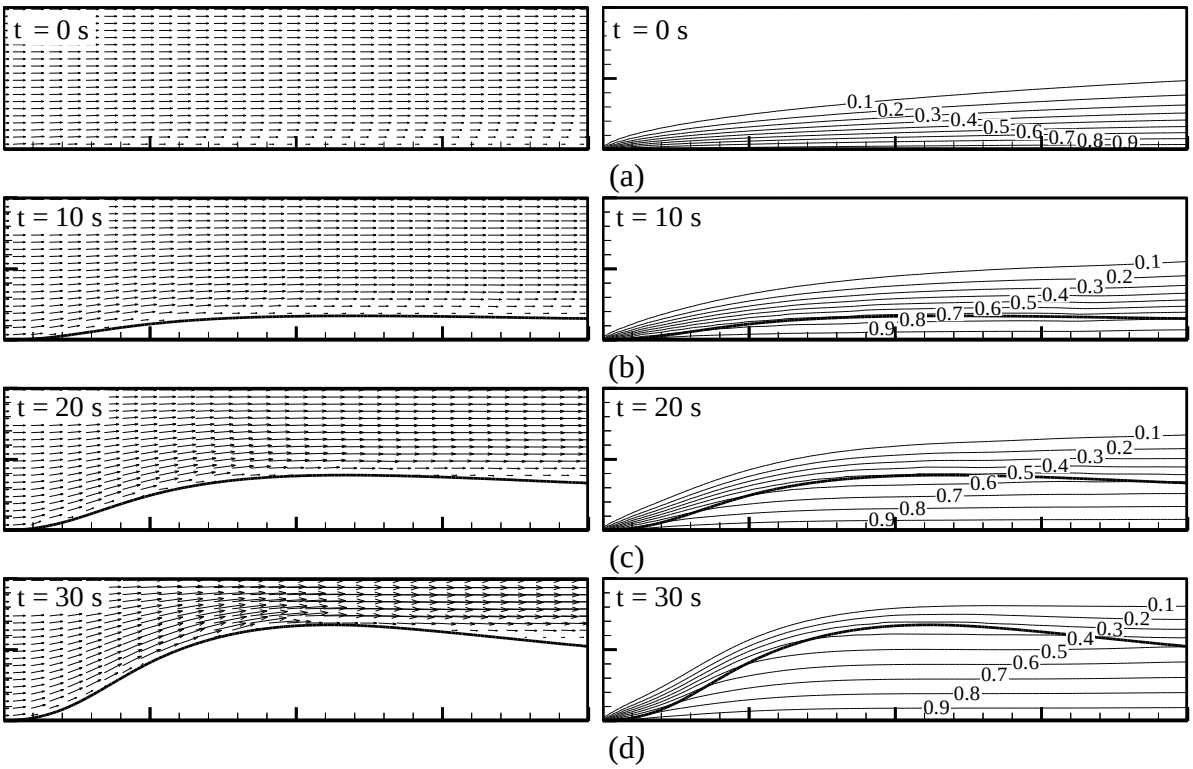

Fig. 8 Dimensionless velocity and temperature fields for the case of Re = 500, Pe = 15.825, α^* = 2 and Pr = 0.214 in the fouled channel at (a) t = 0, (b) t = 10 s, (c) t = 20 s, and (d) t = 30 s.

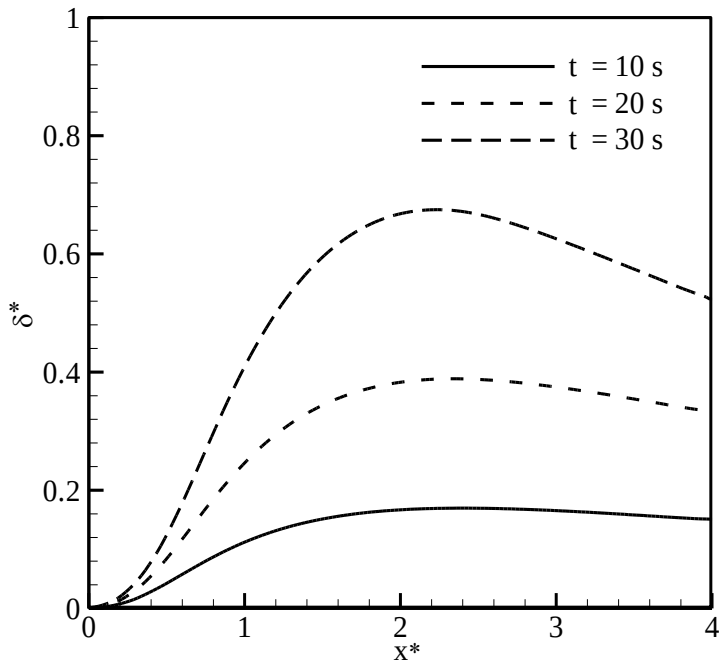

Fig. 9 Evolution of the deposition profile for Re = 500, Pe = 15.825, α^* = 2 and Pr = 0.214.

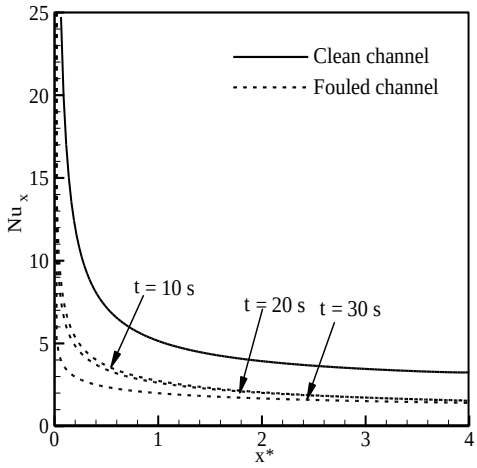

(a)

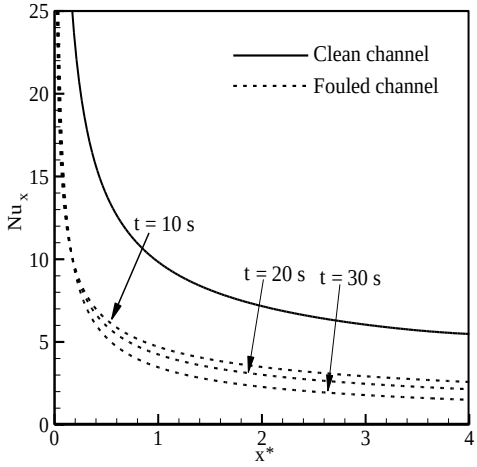

(b)

Fig. 10 Variation of Nu_x along the channel for a clean and a fouled channel for (a) Re = 100, Pe = 3.165 and (b) Re = 500, Pe = 15.825 at α^* = 2 and Pr = 0.214.

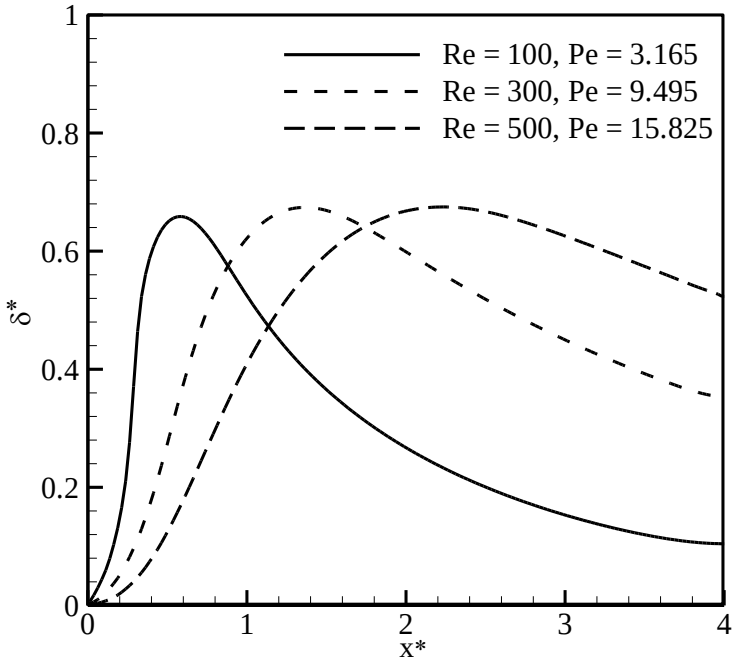

(a)

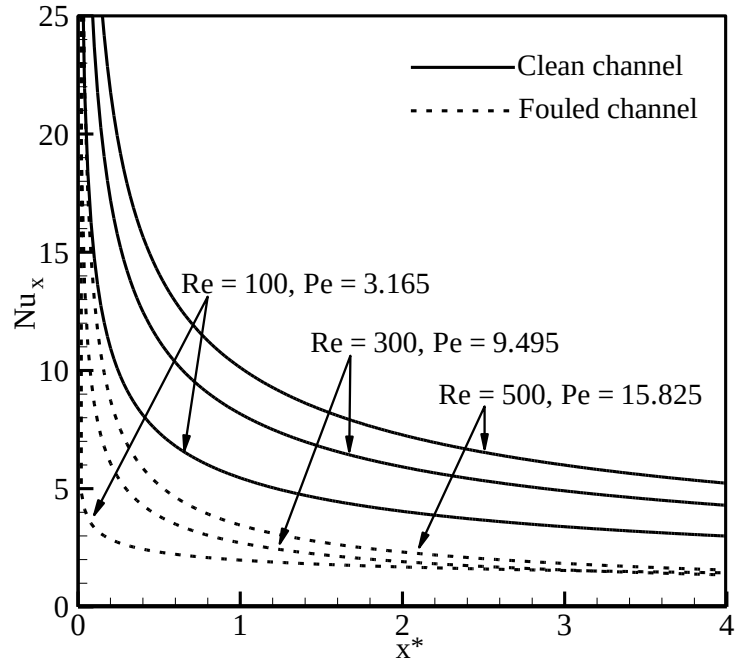

(b)

Fig. 11 Variation of (a) δ^*, and (b) Nu_x under different Re and Pe numbers at t = 30 s under α^* = 2 and Pr = 0.214.

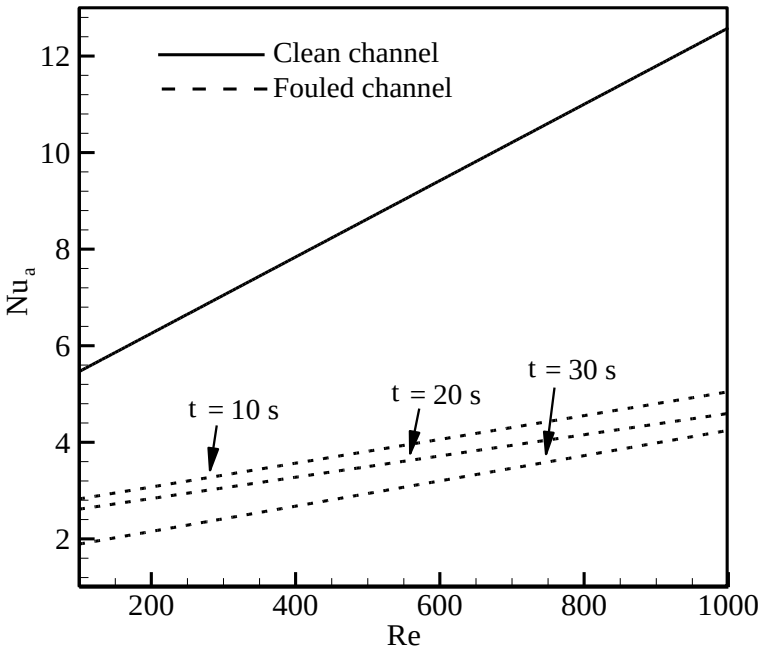

Fig. 12 Variation of Nu_a at different Re and Pe numbers at $\alpha^* = 2$ and Pr = 0.214.

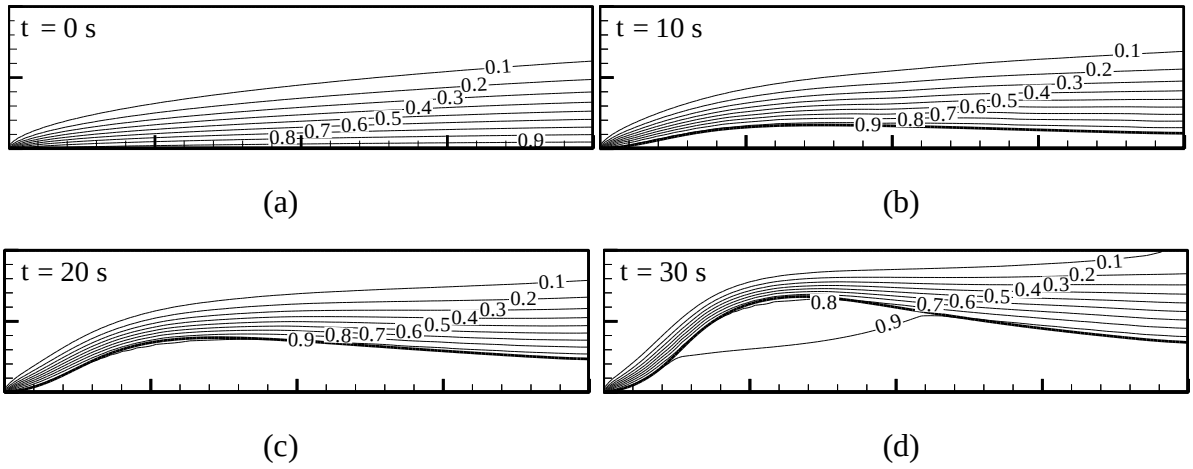

Fig. 13 Dimensionless temperature fields under Re = 300, Pe = 9.495, α^* = 20 and Pr = 0.214 in the fouled channel at (a) t = 0, (b) t = 10 s, (c) t = 20 s, and (d) t = 30 s.

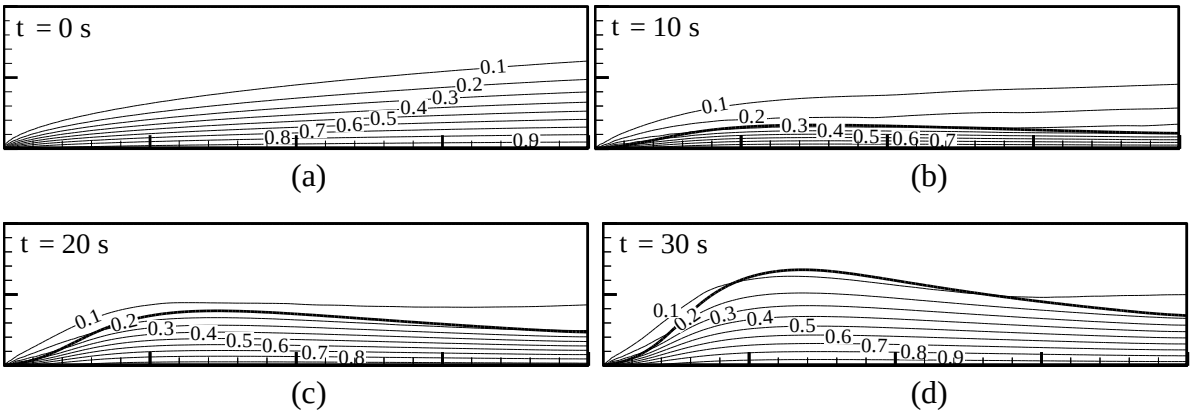

Fig. 14 Dimensionless temperature fields under Re = 300, Pe = 9.495, α^* = 0.2 and Pr = 0.214 in the fouled channel at (a) t = 0, (b) t = 10 s, (c) t = 20 s, and (d) t = 30 s.

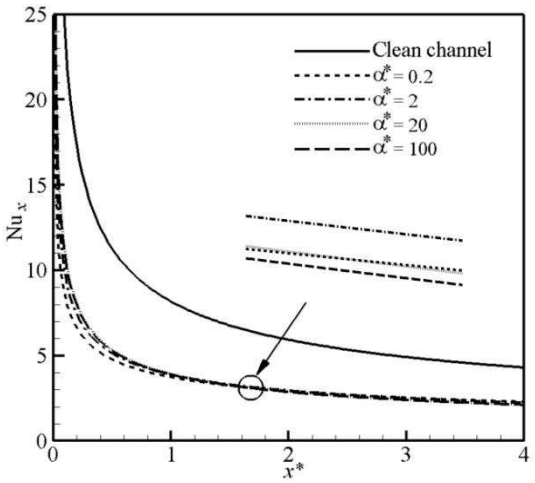

(a)

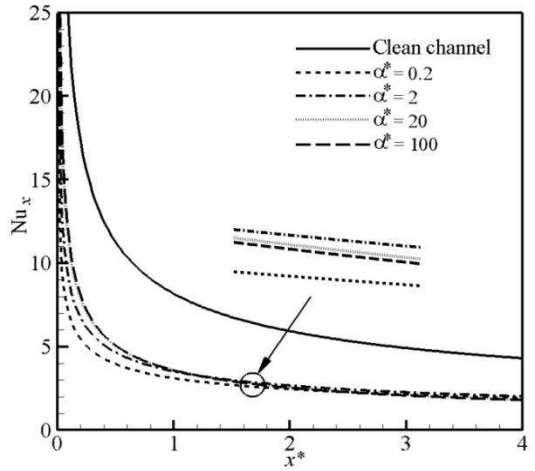

(b)

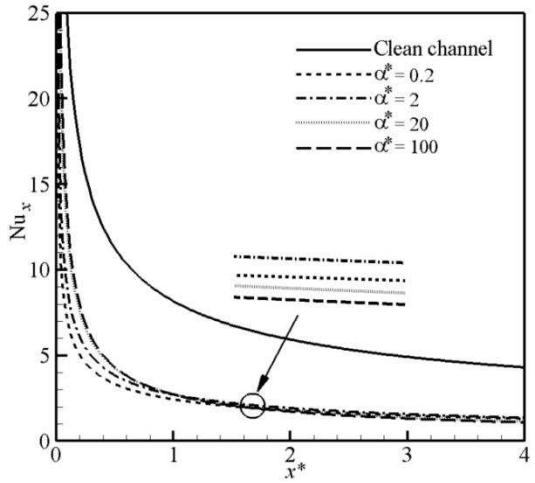

(c)

Fig. 15 Variation of Nu_x along the channel for a clean and a fouled channel at Re = 300, Pe = 9.495 and Pr = 0.214 under different α^* (a) t = 10 s, (b) t = 20 s and (c) t = 30 s.

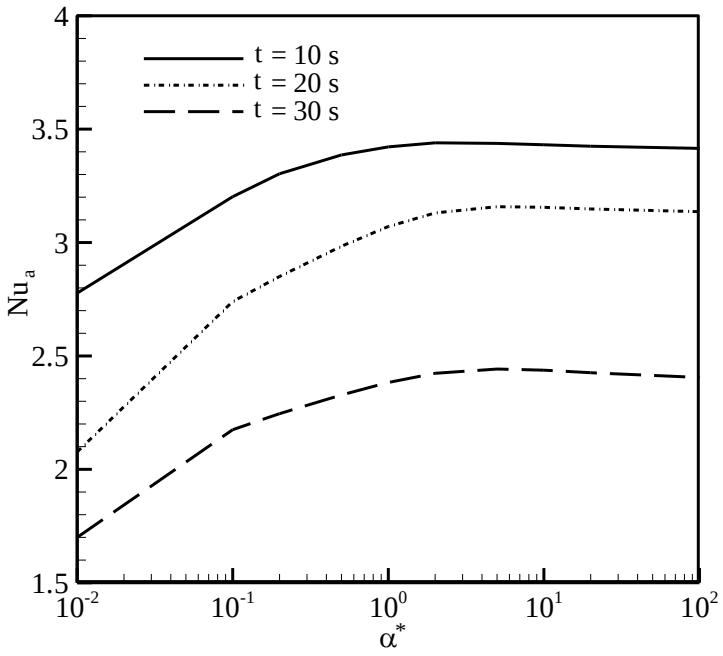

Fig. 16 Variation of Nu_a for different α^* at Re = 300, Pe = 9.495 and Pr = 0.214.

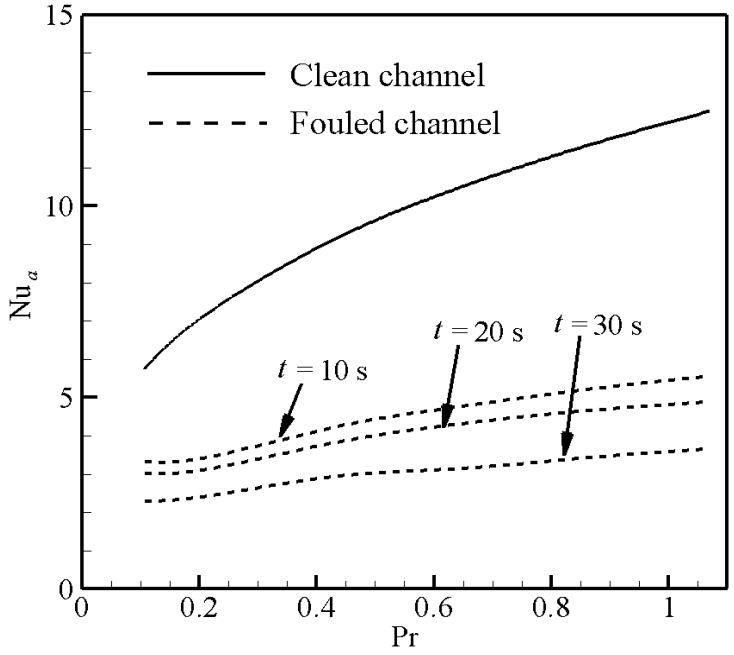

Fig. 17 Variation of Nu_a for different Pr numbers at Re = 300, Pe = 9.495 and $\alpha^* = 2$.